

See discussions, stats, and author profiles for this publication at: <https://www.researchgate.net/publication/263979791>

# Steering Fluorescence Emission with Metal-Dielectric-Metal Structures of Au, Ag, and Al

ARTICLE *in* THE JOURNAL OF PHYSICAL CHEMISTRY C · JULY 2013

Impact Factor: 4.77 · DOI: 10.1021/jp4051066

---

CITATIONS

5

READS

30

---

## 4 AUTHORS, INCLUDING:



Sharmistha Dutta Choudhury

47 PUBLICATIONS 675 CITATIONS

[SEE PROFILE](#)



Ramachandram Badugu

80 PUBLICATIONS 2,491 CITATIONS

[SEE PROFILE](#)



Joseph R Lakowicz

University of Maryland Medical Center

878 PUBLICATIONS 42,292 CITATIONS

[SEE PROFILE](#)

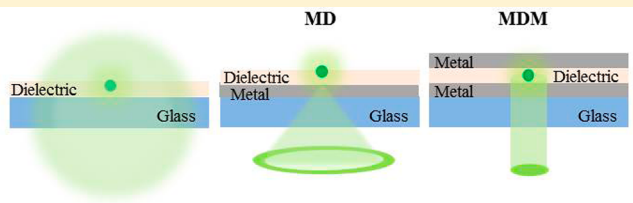
# Steering Fluorescence Emission with Metal-Dielectric-Metal Structures of Au, Ag, and Al

Sharmistha Dutta Choudhury\*,† Ramachandram Badugu,‡ Krishanu Ray,‡ and Joseph R. Lakowicz\*,‡

†Radiation & Photochemistry Division, Bhabha Atomic Research Center, Mumbai 400085, India

‡Center for Fluorescence Spectroscopy, Department of Biochemistry and Molecular Biology, University of Maryland Baltimore, 725 West Lombard Street, Baltimore, Maryland 21201, United States

**ABSTRACT:** Directional control over fluorescence emission is important for improving the sensitivity of fluorescence based techniques. In recent years, plasmonic and photonic structures have shown great promise in shaping the spectral and spatial distribution of fluorescence, which otherwise is typically isotropic in nature and independent of the observation direction. In this work we have explored the potential of metal-dielectric-metal (MDM) structures composed of Au, Ag, or Al in steering the fluorescence emission from various probes emitting in the NIR, visible or UV/blue region. We show that depending on the optical properties of the metal and the thickness of the dielectric layer, the emission from randomly oriented fluorophores embedded within the MDM substrate is transformed into beaming emission normal to the substrate. Agreement of the observed angular emission patterns with reflectivity calculations reveals that the directional emission is due to the coupling of the fluorescence with the electromagnetic modes supported by the MDM structure.



## INTRODUCTION

Fluorescence is a versatile and widely used technique due to its high sensitivity, ease of detection, and rapid response. Most uses of fluorescence depend on the spontaneous emission of photons that occurs nearly isotropically in all directions. This means that the fluorescence properties are mostly independent of the observation direction, except for special cases such as systems with oriented dipoles. The omnidirectional nature of fluorescence makes it difficult to capture more than about 1% of the total emission with typical detection systems.<sup>1</sup> Higher fluorescence collection efficiencies near 10% are possible but at the expense of complex optics.<sup>2</sup> To improve fluorescence detection capabilities for practical applications, it is desirable to control the direction of emission in a cost-effective manner and preferably to obtain the entire emission as a narrow beam normal to the sample surface.

In recent years, there has been an upsurge in the use of plasmonics and nanophotonics for directing and controlling the flow of optical energy.<sup>3,4</sup> Nanometer scaled structures made of metallic, dielectric, or hybrid materials are being studied to tailor the optical environment surrounding a fluorescent molecule and thereby influence its emission properties.<sup>5–10</sup> For example, nanometallic optical antennas are capable of locally enhancing and directing electromagnetic fields. Curto et al. have demonstrated that quantum dots coupled to a Yagi-Uda nanoantenna can show unidirectional emission.<sup>7</sup> Recently, bright unidirectional emission has been observed from molecules in a nanopore with plasmonic corrugations.<sup>8,9</sup> Jun et al. have shown electrical control over the beaming emission from a plasmonic cavity coupled with a miniature grating structure.<sup>10</sup> All of these complex and precise material

architectures require the use of nanofabrication techniques such as electron beam or focused ion beam lithography that are limited by high manufacturing costs, low throughput, and small surface areas. To overcome some of these limitations, recently Ding et al. proposed nanosphere lithography to develop large area self-assembled plasmonic-photonic crystals for spectral and directional reshaping of fluorescence.<sup>11</sup> Some years back, we showed that the radiation patterns of fluorophores can be altered by coupling the emission with the surface plasmon resonance of thin metal films deposited on a glass slide.<sup>12–15</sup> These films can be prepared with standard thermal evaporation methods and do not require special handling techniques. In this phenomenon, known as surface-plasmon-coupled emission (SPCE), fluorophores placed in the vicinity of the metal films can radiate into the substrate at specific directions dictated by the surface plasmon resonance conditions of the metal film. Interestingly, the fluorescence emission carries the polarization and dispersion characteristics of the surface plasmon mode. As the thickness of the fluorophore bearing dielectric layer above the metal film is increased, the fluorescence emission couples with additional waveguide modes present in the dielectric layer, leading to polarized emission at several different angles.<sup>14,16</sup>

Encouraged by the growing popularity and widespread use of SPCE,<sup>17–20</sup> recently, we have considered the effects of an additional metal layer above the single metal-dielectric (MD) surface, leading to a metal-dielectric-metal (MDM) structure.<sup>21</sup> For a fluorophore embedded in a dielectric layer sandwiched

Received: May 23, 2013

Revised: July 1, 2013

Published: July 2, 2013



between two thin metal films, the situation is in many ways different from the simple single thin metal film case. For MDM structures, the interactions between the two metallic surfaces can lead to the creation of coupled surface plasmon modes and photonic modes of different orders.<sup>22</sup> From our recent study on such MDM structures composed of Ag, we have found that for particular thicknesses of the dielectric layer, the coupling of the fluorescence to the Fabry–Perot modes can lead to the channelling of fluorescence emission in a direction normal to the MDM substrate. The observation of beaming emission from such simple structures is an interesting result and can have many important applications. We have shown that these MDM structures, with spatial control over the fluorescence emission, can be readily adapted for multiple uses, as in microarray formats, for directional fluorescence studies of multiple probes, or for biosensing applications.<sup>21</sup> We realized that it would be possible to tailor the light matter interactions in a simple and flexible manner by changing the design parameters of the MDM structure. The nature and thicknesses of the metallic or dielectric layer could be varied to suit our requirements and according to the emission range of the fluorophore. In this paper we consider the effects of three different metals, Au, Ag, and Al, in altering the directional characteristics of fluorescence emission in the respective MDM structures. It is expected that due to the different wavelength dependent optical properties of Au, Ag, and Al, these metals can be used to tune the fluorescence properties of fluorophores emitting in the NIR, visible, or UV/blue region, respectively.<sup>15</sup> Accordingly, we have chosen three fluorescent probes emitting in the above spectral regions, and we present the radiation patterns and emission characteristics of these molecules in the corresponding, wavelength-compatible MDM structure.

## EXPERIMENTAL METHODS

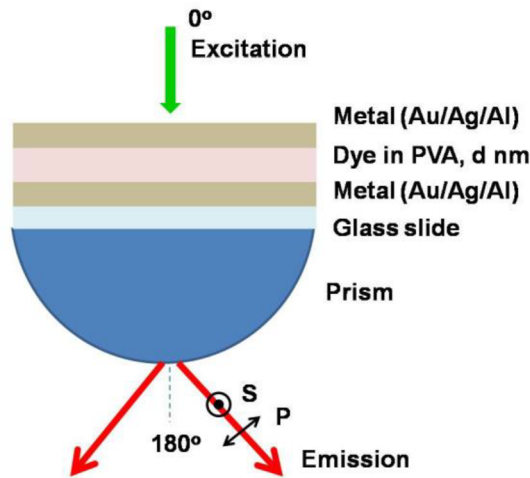
**Materials.** The metals, Au, Ag, and Al (purity 99.999%), poly(vinylalcohol) (PVA, MW 13000–23000), Nile Blue (NB), Fluorescein (Fl), and 7-amino-4-methylcoumarin (AMC) were purchased from Sigma-Aldrich. Glass microscope slides were obtained from VWR.

**Preparation of the MDM Substrates.** The glass slides were cleaned by soaking in “piranha solution” overnight, followed by washing thoroughly with distilled deionized water, and dried with air stream. Metallic films (thickness ~50 nm for Au, Ag, and 15 nm for Al) were deposited on the cleaned glass slides using an Edwards Auto 306 vacuum evaporation chamber under high vacuum ( $<5 \times 10^{-7}$  Torr). The deposition rate (~1.0 nm/min) was adjusted by the filament current and the thickness of the deposited film was measured with a built-in quartz crystal microbalance. The surface of the metal film (Au, Ag, or Al) was then spin-coated (at 3000 rpm) with an aqueous solution of PVA, containing the fluorophores (~100  $\mu\text{M}$ , NB in case of Au, Fl for Ag, and AMC for Al). The weight percentages of PVA were varied to obtain various thicknesses of the dielectric, PVA layer. The film thickness corresponding to different PVA concentrations and the calibration curve for the same is discussed in detail in our previous papers.<sup>14,21</sup> We refer to this PVA coated metal film as a MD structure. After the PVA layer, a second metallic layer (50 nm) was added by thermal vapor deposition to get the final Au-PVA(NB)-Au, Ag-PVA(Fl)-Ag, or Al-PVA(AMC)-Al MDM substrates. The second metal layer was not deposited for the MD substrates.

**Fluorescence Measurements.** The MDM (and MD) samples on glass slides were fixed to a hemicylindrical quartz

prism using glycerol as a refractive index matching fluid. The prism along with the attached sample was placed on a precise rotary stage that allows excitation and observation at any angle relative to the vertical axis of the cylinder. The samples were illuminated in the reverse Kretschmann configuration, from the air side, which is distal from the prism, and normal to the sample surface. For the MDM substrates, excitation was through the top metal film. A schematic of the illumination geometry is presented in Scheme 1. The emission was collected

**Scheme 1. Schematic of the MDM Substrate and the Illumination Geometry (Reverse Kretschmann) Used in the Present Study<sup>a</sup>**



<sup>a</sup>The substrate was attached to the prism with glycerol for refractive index matching. The emission was collected at different angles using an optical fiber. The S- and P-polarizations of the emission are indicated in the figure.

with an Ocean Optics optical fiber (diameter 1 mm and NA 0.22). The output of the fiber was connected to a spectrofluorometer (Ocean Optics SD2000) for recording the emission spectra and to a TCSPC instrument (PicoQuant, Fluotime 100) for time-resolved measurements. Pulsed laser diodes from Picoquant (100 ps, 40 MHz) were used as the excitation sources for all studies. The excitation wavelengths were as follows: 635 nm for Au-PVA(NB)-Au, 470 nm for Ag-PVA(Fl)-Ag, and 375 nm for Al-PVA(AMC)-Al. The excitation light was passed through laser cleanup filters and the emission was observed through suitable long pass filters to suppress any scattered light. The S- and P-polarized emissions were observed by changing the polarizer orientation in front of the fiber optic cable. The emission intensities at each observation angle were obtained by integrating the area under the emission spectra at the corresponding angles. Lifetimes were estimated by fitting to a  $\chi^2$  value of less than 1.2 and a residual trace that was symmetrical about the zero axis. For the photographs, the samples were attached to a hemispherical prism instead of a hemicylinder.

**Reflectivity Calculations.** The reflectivity calculations were performed using the TF Calc. software package (Software Spectra, Inc., Portland, Oregon) that is used to design multilayer optical filters. Light was considered to be incident on the metal film through the prism (Kretschmann configuration). For simplicity, the prism and the glass slide were considered as a single phase with the same refractive index

( $n = 1.52$ ). The angle-dependent reflectivity spectra were calculated using appropriate optical constants of the metals for the particular substrate configuration and the wavelength corresponding to the emission maxima of the respective probe. The thickness of the PVA layer (refractive index,  $n = 1.52$ ) was varied during the calculations to match the measured angular emissions with the respective MDM structures. We found reasonable agreement between the observed angular emissions and the calculated angles and polarizations of the reflectivity minima. The calculated PVA thicknesses were also consistent with the known film thicknesses at various weight percentages of PVA.

## ■ RESULTS AND DISCUSSION

The optical and reflective properties of metals depend on the interplay of the incident light frequency, electron mobility, and the underlying absorption bands present in the metal. These properties are described by the complex, frequency-dependent permittivity or dielectric constant given as

$$\epsilon_m = \epsilon_r + i\epsilon_{im} \quad (1)$$

that is related to the complex refractive index by the relation

$$n_m = n_r + i n_{im} = \sqrt{\epsilon_m} \quad (2)$$

The subscripts indicate the real (r) and imaginary (im) components. Figure 1 shows the wavelength dependence of the

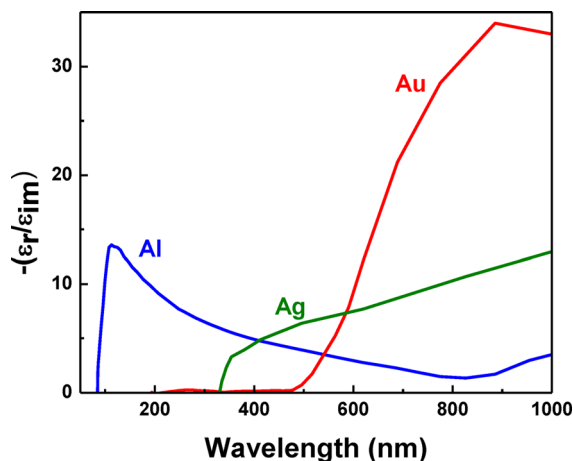


**Figure 1.** Wavelength dependence of the ratio between the real and imaginary components of the complex dielectric constants,  $\epsilon_m = \epsilon_r + i\epsilon_{im}$ , of Au, Ag, and Al. The optical constants for the metals have been taken from ref 23.

ratio between the real and imaginary parts of the dielectric constants ( $-\epsilon_r/\epsilon_{im}$ ) for Au, Ag, and Al.<sup>23</sup> This figure can be used to gather an intuitive understanding about the reflectivity spectra and plasmonic properties of the metals. In general, as seen for Au, Ag, and Al in Figure 1, the real part of the dielectric constant of metals becomes increasingly negative with increase in wavelength. This corresponds to the more complete response of the electron oscillations in the metal with decreasing frequency of the incident light. The imaginary part of the dielectric constant is positive and corresponds to the absorption of light by the metal. The imaginary component increases for wavelengths where the absorption becomes higher. This can be seen in Figure 1 by the sharp decrease in ( $-\epsilon_r/\epsilon_{im}$ ) below about 120 nm for Al, about 350 nm for Ag, and about 500 nm for Au, corresponding to the onset of

interband transitions for these metals. Since Al does not have an intrinsic absorption until the deep UV region, it serves as a very suitable material for coupling with the emission from fluorophores emitting in the UV/blue region.<sup>24</sup> Ag can be used for fluorophores emitting from about 350 to 800 nm, while Au is more suitable for the NIR region. Au has some advantages over Ag, owing to its long-term chemical stability and favorable surface chemistry.<sup>25</sup>

Keeping the above optical properties in mind, we have chosen three representative fluorophores, Nile blue (NB, emission maximum around 670 nm), Fluorescein (Fl, emission maximum around 515 nm), and 7-amino-4-methylcoumarin (AMC, emission maximum around 445 nm), to study their emission properties with MDM substrates of Au, Ag, and Al, respectively. Figure 2 shows the emission spectra of these

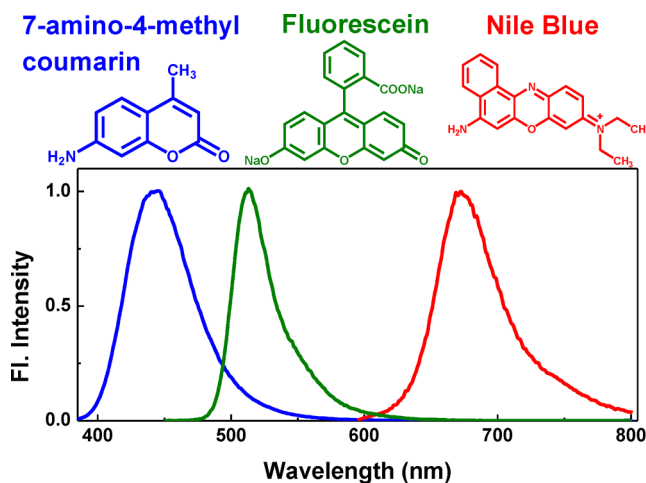


**Figure 2.** Chemical structures and normalized emission spectra of the fluorophores, 7-amino-4-methylcoumarin (AMC), Fluorescein (Fl), and Nile blue (NB).

probes along with their chemical structures. For the present study, we have avoided the deep UV region because that requires additional changes in the optical components and excitation source. As described in the Experimental Methods section, the MDM samples were prepared by thermal vapor deposition of Au, Ag, or Al films, spin coating a layer of PVA containing the appropriate fluorescence probe and followed by depositing another layer of the same metal. Angle dependent fluorescence was recorded by exciting the samples through the top metal surface in the reverse Kretschmann configuration, and collecting the emission through the prism with an optical fiber mounted on a rotation stage (Scheme 1).

The angular emission patterns observed for NB embedded in the Au-PVA-Au substrate with different thicknesses of PVA are shown in Figure 3. No emission is observed in the MDM substrate below a certain thickness (~160 nm) of the PVA dielectric layer. At a PVA film thickness of about 160 nm, the emission is seen to be highly directional and most of the emission is concentrated in a narrow beam normal to the substrate (Figure 3A). With increasing film thickness, the emission pattern changes gradually with the S- and P-polarized emissions appearing at definite angles. On reaching a PVA thickness about 380 nm, the beaming emission is observed again and is also accompanied by an S-polarized component at a different angle (Figure 3D).

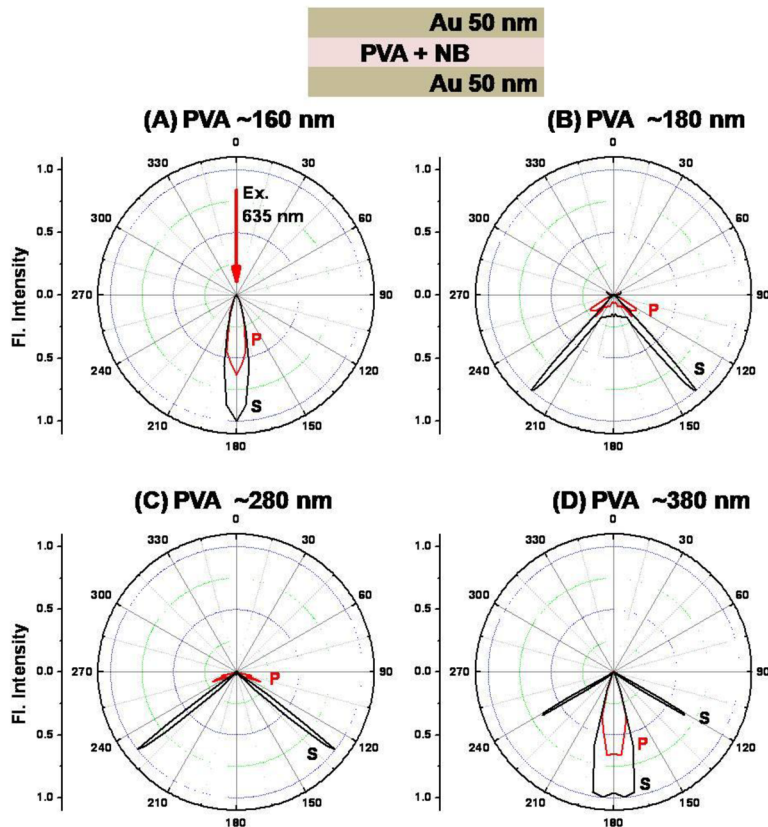


**Figure 3.** Angular distributions of the fluorescence intensities for S- (black) and P-polarized (red) emission from NB, with different PVA film thicknesses in the Au-PVA-Au MDM substrates (schematic in the top panel).

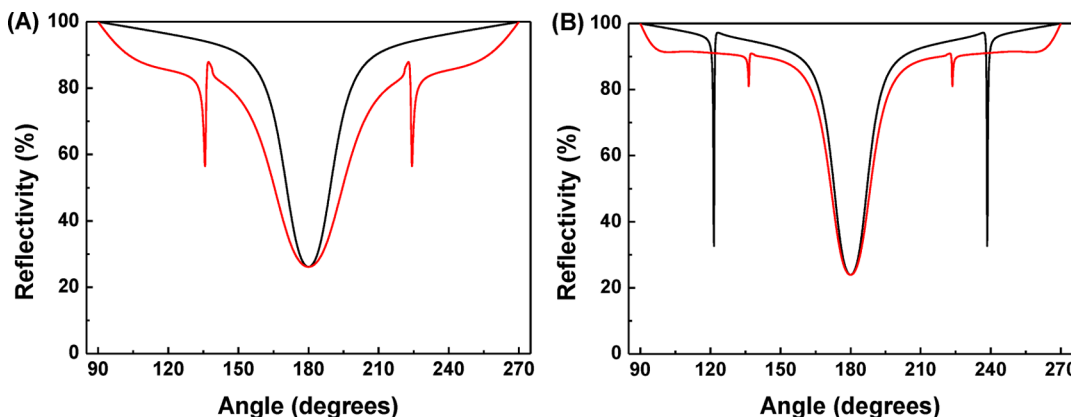


**Figure 4.** Calculated reflectivity curves for 670 nm S- (black) and P-polarized (red) light for Au-PVA-Au with PVA thickness 161 nm (A) and 384 nm (B).

Figure 4 shows the calculated angle-dependent reflectivity curves for 670 nm light (corresponding to the emission maximum of NB), in the Au-PVA-Au substrates with different assumed values for the PVA thickness. For the calculations, the illumination was considered through the prism, which is called the Kretschmann configuration. The calculated reflectivity curves are found to be in close agreement with the angular emission patterns of NB observed with the MDM substrates. Specifically, when we consider a PVA thickness of 161 nm, a dip in reflectivity is obtained for light normal to the surface. This corresponds with the observed beaming emission for the Au-PVA-Au MDM substrate having PVA thickness about 160 nm (Figure 3A). The reflectivity calculation also shows smaller

and sharper dips for P-polarized light around 136° and 224°. However, this P-polarized emission is weak and cannot be clearly detected under the experimental conditions. This weak signal may be due to the narrow range of wavelengths which couples with this sharp resonance. Considering a PVA thickness of 384 nm, the simulated reflectivity curve shows a minimum at 180° along with sharp minima for S-polarized light at 120° and 240°. These match very well with the emissions observed normal to the surface and at ~120° and 240° for the Au-PVA-Au substrate shown in Figure 3D. Slight differences in the PVA thickness obtained from the reflectivity calculations and the known film thickness of PVA are possibly due to local variations in thickness during film preparation by spin

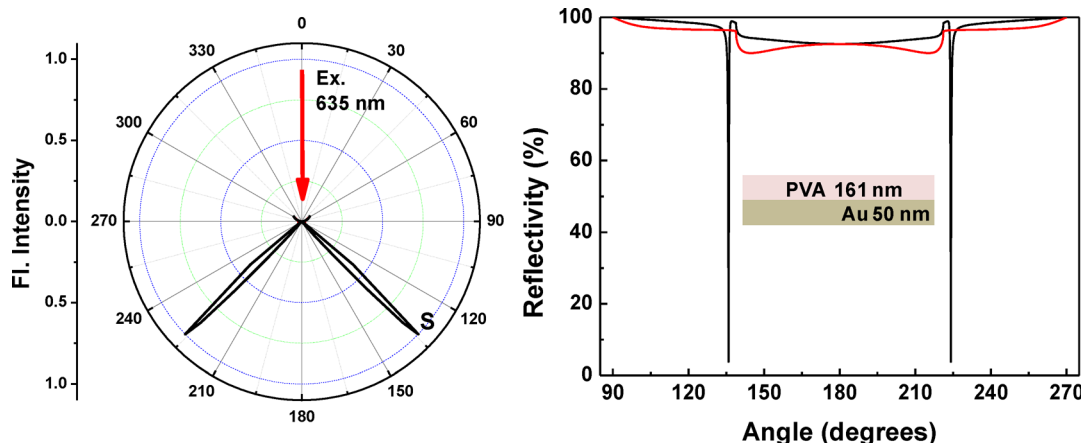


**Figure 5.** Measured angular distributions of the fluorescence intensities for S- (black) and P-polarized (red) emission of NB in the Au-PVA substrate with PVA thickness about 160 nm. The calculated reflectivity curve for this sample configuration at a PVA thickness of 161 nm is shown in the right panel.

coating.<sup>21</sup> Moreover, it should be remembered that a fluorophore emits with a finite bandwidth, so that in reality the angular emission distributions are expected to be wider than the theoretically calculated values for a single emission wavelength. It is also important to mention that the positions and polarizations of the reflectivity minima are very sensitive to even slight changes (nanometer range) in the thicknesses of the layers.

The reflectivity spectra calculated on the basis of the transfer matrix formalism using the commercially available software, TF Calc., can be thought to correspond with the resonances for the various electromagnetic modes present in the MDM structure. For example, for a thin metal film illuminated by light of a certain wavelength ( $\lambda$ ) through a glass prism, the calculated reflectivity minimum appears at a certain specific angle ( $\theta_{sp,\lambda}$ ), beyond the critical angle for the system. This reflectivity dip is in fact related to the excitation of the surface plasmon resonance mode of the metal film for that particular wavelength and angle. When a fluorophore having an emission wavelength of  $\lambda$  is placed in the vicinity of this metal film, the emission through the substrate is observed at the same specific angle,  $\theta_{sp,\lambda}$ , due to the near-field coupling of the emission with the surface plasmon mode.<sup>12</sup> Thus, the correlation between the calculated reflectivity spectra of the Au-PVA-Au substrate and the experimentally observed emission patterns with this substrate implies that the fluorescence emission from NB is being mediated by the electromagnetic modes present in the MDM substrate. Consequently, the fluorescence emission bears the characteristic properties of these modes. However, it is quite difficult to make accurate predictions of the intensity at a given angle and the coupling of fluorophores with the various modes propagating in the substrate, because additional considerations have to be made for the orientation of the fluorophore dipoles and the quenching effects of the metal at very close metal-fluorophore distances.

The conversion of the isotropic emission from the randomly oriented probes to the beaming emission normal to the sample surface in certain Au-PVA-Au substrates is thought to be due to the coupling of the emission to Fabry-Perot modes.<sup>21</sup> The Fabry-Perot modes can be understood as the constructive interference of waves propagating upward and downward in the PVA layer in a direction perpendicular to the metal-dielectric interface. The resonance conditions are satisfied when

$$\lambda_{\text{resonance}} = 2d_{\text{effective}}/m \quad \text{and}$$

$$d_{\text{effective}} = nd_{\text{PVA}} + d_{\text{phase-change}} \quad (3)$$

Here,  $m$  is an integer,  $n$  is the refractive index of PVA ( $n = 1.52$ ), and  $d_{\text{effective}}$  is the effective thickness of the MDM cavity. The effective thickness comprises  $d_{\text{PVA}}$ , the distance between the Au films determined by the physical thickness of the PVA layer, and  $d_{\text{phase-change}}$  that arises due to the phase shift upon reflection at the Au-dielectric interfaces.<sup>26,27</sup> For ideal reflecting mirrors, the phase change on reflection is  $\pi$ , and in this case  $d_{\text{effective}} = nd_{\text{PVA}}$ . Considering an emission wavelength of 670 nm (corresponding to the emission maximum of NB) and perfect reflecting mirrors, the first resonance condition ( $m = 1$ ) would be satisfied at an effective thickness ( $d_{\text{effective}}$ ) of 335 nm or at a PVA thickness of about 220 nm. In the present case, the beaming emission is observed for the Au-PVA-Au substrate which has a PVA thickness ( $d_{\text{PVA}}$ ) of about 160 nm. This implies that the phase change due to reflection from the two Au surfaces in the MDM substrate contributes significantly toward the effective thickness ( $d_{\text{phase-change}}$ ). The second Fabry-Perot resonance mode for this MDM substrate is expected at a dielectric thickness of about 380 nm. This matches quite well with the beaming emission observed in the Au-PVA-Au sample in Figure 3D. The Fabry-Perot mode cannot exist for MDM structures with thickness lower than a critical value ( $d_{\text{critical}} < \lambda_{\text{resonance}}/2m$ ). This explains why no emission is observed from NB in the Au-PVA-Au substrates for PVA thicknesses less than about 160 nm.

To understand and compare the emission patterns in the MDM substrate with that observed with a metal-dielectric substrate (MD), we have also studied the emission from NB in a 160-nm-thick PVA film above a single 50 nm Au film (Au-PVA). The angular emission plots and the calculated reflectivity curves for NB fluorescence in this substrate are shown in Figure 5. In this case, the emission is S-polarized and most of the emitted light is observed at an angle of  $\sim 136^\circ$  (and  $\sim 224^\circ$  due to symmetry). The minimum in the calculated reflectivity curve also appears at similar angles for S-polarized light of wavelength 670 nm and for PVA thickness of 161 nm. With the MD substrate, no emission is observed in a direction normal to the substrate surface for any thickness of the PVA layer. This is the typical result with SPCE.

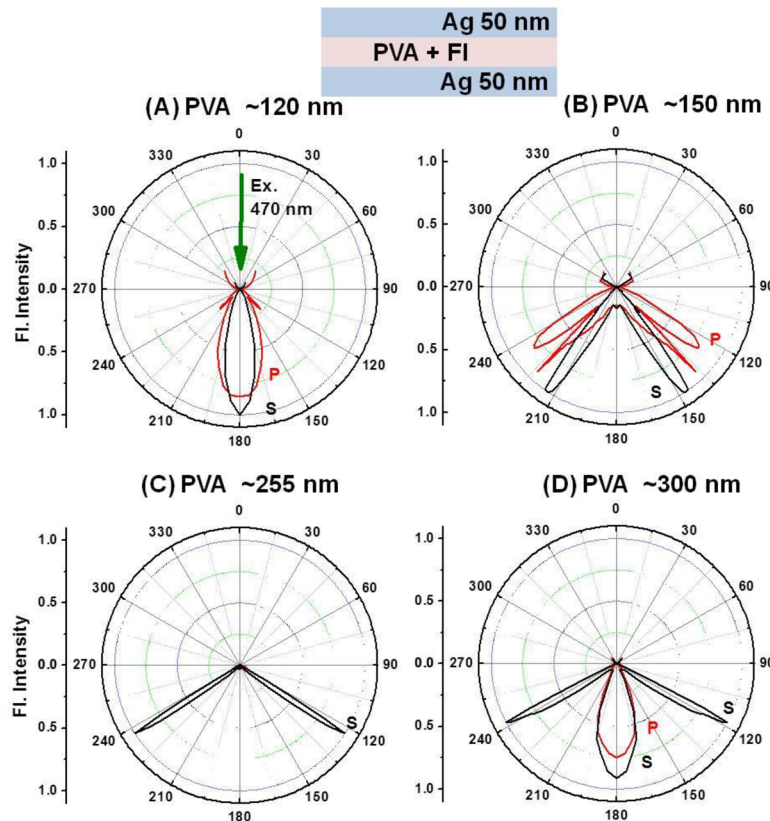


**Figure 6.** Angular distributions of the fluorescence intensities for S- (black) and P-polarized (red) emission from Fl, with different PVA film thicknesses in the Ag-PVA-Ag MDM substrates (schematic in the top panel).

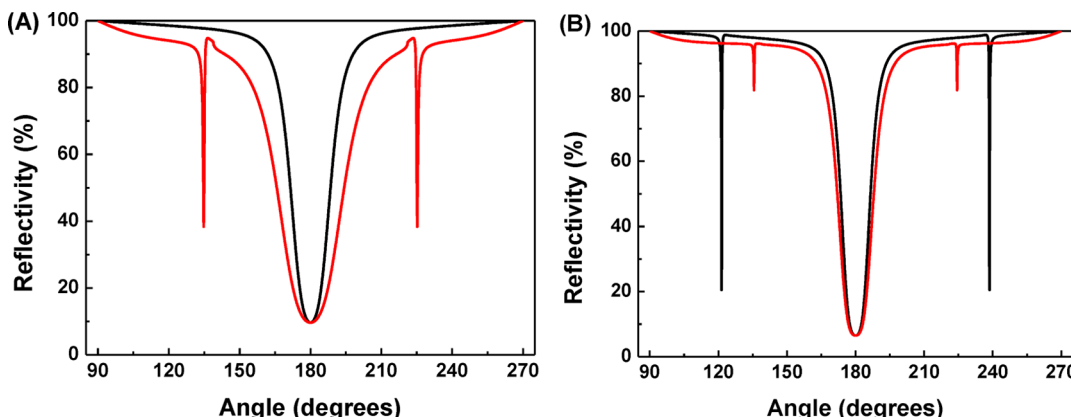


**Figure 7.** Calculated reflectivity curves for 515 nm S- (black) and P-polarized (red) light for Ag-PVA-Ag with PVA thickness 119 nm (A) and 294 nm (B).

We carried out similar angle dependent emission measurements for Fl (emission maximum around 515 nm) embedded in Ag-PVA-Ag substrates and AMC (emission maximum around 445 nm) embedded in Al-PVA-Al substrates, with varying PVA thicknesses. Characteristic radiation patterns were observed in each case. The beaming emission was obtained at different PVA thicknesses depending on the emission wavelength and the type of metal, which is consistent with eq 3. For Ag-PVA-Ag, the beaming emission appears at a PVA thickness of about 120 nm (Figure 6A) corresponding to the coupling with the first Fabry-Perot mode. The second beaming emission appears at a PVA thickness of about 300 nm (Figure 6D) that matches well with the thickness requirement for

propagation of the second order Fabry-Perot mode. The other emissions observed at  $\sim 135^\circ$  and  $\sim 225^\circ$  (P-polarized) in Figure 6A and  $\sim 120^\circ$  and  $\sim 240^\circ$  (S-polarized) in Figure 6D are possibly due to the coupling of the fluorescence with the additional electromagnetic modes present in the MDM substrate. These experimental observations are consistent with the theoretically simulated reflectance curves at these thicknesses and for a wavelength of 515 nm (Figure 7). Comparison with the corresponding MD substrate composed of Fl embedded in a 120-nm-thick PVA film on a single 50 nm Ag layer, shows no beaming emission. Instead, the emission is S-polarized and appears at  $\sim 135^\circ$  and  $\sim 225^\circ$ , which is in

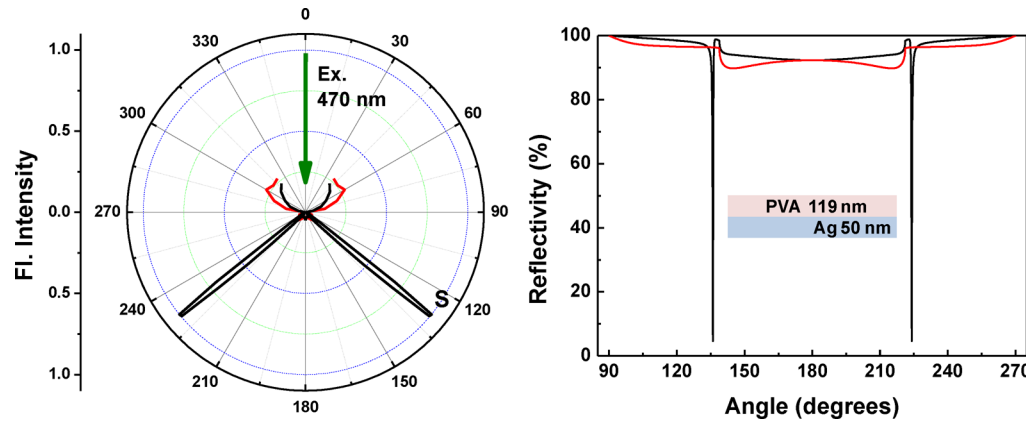


**Figure 8.** Measured angular distributions of the fluorescence intensities for S- (black) and P-polarized (red) emission of Fl in the Ag-PVA substrate with PVA thickness about 120 nm. The calculated reflectivity curve for this sample configuration at a PVA thickness of 119 nm is shown in the right panel.

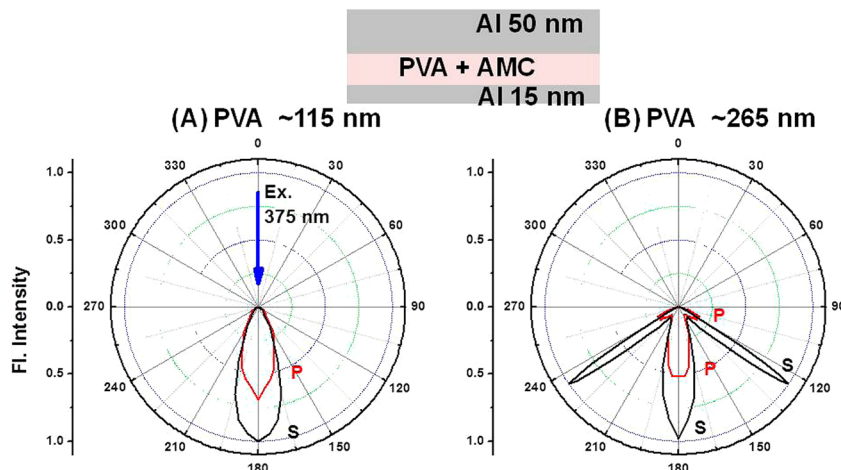


**Figure 9.** Angular distributions of the fluorescence intensities for S- (black) and P-polarized (red) emission from AMC, with different PVA film thicknesses in the Al-PVA-Al MDM substrates (top panel).

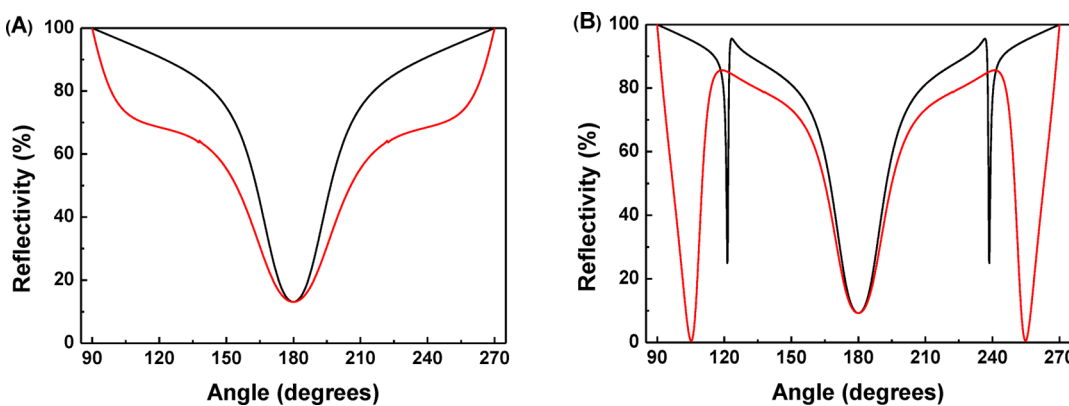


**Figure 10.** Calculated reflectivity curves for 445 nm S- (black) and P-polarized (red) light for Al-PVA-Al substrates with PVA thickness 115 nm (A) and 264 nm (B).

accordance with the reflectivity calculations for the MD structure (Figure 8).

In the above two cases of Au-PVA-Au and Ag-PVA-Ag, the best emission intensities were observed with a metal film thickness of about 50 nm, for both the top and bottom layers. However, in the case of MDM substrates of Al, better emission intensities were obtained with a much lower thickness of 15 nm

for the bottom Al layer. The beaming emission for AMC in Al-PVA-Al substrates with PVA thicknesses corresponding to the first and second Fabry-Perot modes ( $\sim 115$  nm and  $\sim 265$  nm, respectively) are presented in Figure 9. The corresponding reflectivity curves are shown in Figure 10. For the MDM configuration corresponding to the resonance condition of the second order Fabry-Perot mode, emission is observed at two

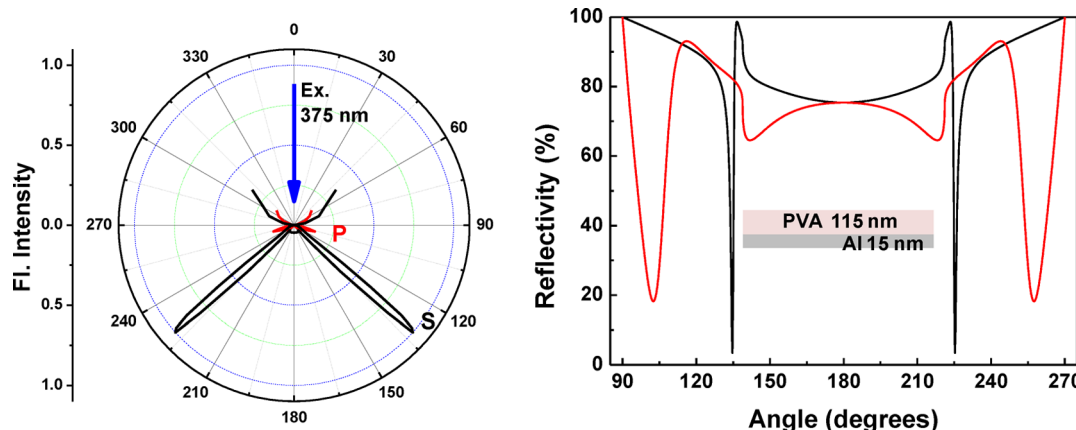


**Figure 11.** Measured angular distributions of the fluorescence intensities for S- (black) and P-polarized (red) emission of AMC in the Al-PVA substrate, having PVA thickness about 115 nm. The calculated reflectivity curve for this sample configuration at a PVA thickness of 115 nm is shown in the right panel.

other angles in addition to the beaming emission normal to the surface (Figure 9B). The S-polarized emission appears at about  $\sim 120^\circ$  (and  $\sim 240^\circ$ ). This feature is similar to that observed in the case of the MDM substrates of Au and Ag (Figures 3D and 6D). With Al-PVA-Al, however, additional P-polarized emission can be seen around  $105^\circ$  (and  $\sim 255^\circ$ ). It is also observed that the angular spread of the beaming emission is quite large in the case of Al-PVA-Al compared to that obtained in the Au-PVA-Au and Ag-PVA-Ag substrates. These variations are attributed to the differences in the properties of the electromagnetic modes supported by the MDM structures composed of different metals. Comparison between the radiation patterns of AMC in the MDM substrate with the MD substrate again shows that there is no beaming emission in the latter case. With the Al-PVA MD substrate, the emission is observed at  $\sim 135^\circ$  (and  $\sim 225^\circ$ ) for S-polarization and at  $\sim 105^\circ$  (and  $\sim 255^\circ$ ) for P-polarization. Reflectivity dips for this substrate are also found with the same polarizations and at similar angles (Figure 11). It is worthwhile to mention that, while the Al MDM substrates were stable for a few days, the MDM substrates with Au and Ag were quite stable for about a month.

The differences in the emission patterns observed with an MDM substrate and an MD substrate can be nicely visualized from the fluorescence images obtained for a fluorophore embedded in these two substrates. Figure 12 shows the real

color photographs of the emission patterns of Fl in MD and MDM substrates. While the emission of Fl embedded in the Ag-PVA MD substrate generates a ring of fluorescence, the emission of Fl in the Ag-PVA-Ag MDM substrate, having the same PVA thickness of  $\sim 120$  nm, generates a distinct fluorescence spot. From Figure 8, we expect the emission from the MD substrate with 120 nm PVA to be S-polarized. For S-polarized light, the polarization direction is tangential around the ring of emission and is independent of the azimuthal angle. This tangential polarization can be seen by observing the emission through a polarizer. We arbitrarily chose the vertical direction as S in Figure 12. It is found that the top and bottom portions of the rings cannot be seen when the emission is observed through a vertically oriented polarizer (S). Similarly, the sides of the ring cannot be seen when the emission is observed through a horizontally oriented polarizer (P).<sup>14</sup> In the case of the MDM substrate both the vertically and horizontally polarized light appear normal to the sample surface. So, the emission spot can be observed completely with both horizontal and vertical orientations of the emission polarizer.

Considering that the fluorescence emission from probes within the MDM substrate is being mediated through the electromagnetic modes present in the substrate, it may be expected that the spontaneous emission rates for fluorophores placed within the substrate will be increased due to the alteration in the photonic mode density (Purcell effect).<sup>28</sup> Figure 13 shows the fluorescence intensity decays for the fluorophores placed within MDM substrates of Au, Ag, and Al (substrate configurations corresponding to Figures 3A, 6A, and 9A that show beaming emission). A significant reduction in the fluorescence lifetime of all the probes is observed in the MDM substrates in comparison to the lifetime of the probe in PVA spin coated on glass without any metal layer (Figure 13). The average fluorescence lifetime of NB in Au-PVA-Au is 1.9 ns compared to the average lifetime of 2.4 ns for NB on glass (PVA thickness in each case is 160 nm). Similarly, the average fluorescence lifetime of Fl is 1.6 ns in Ag-PVA-Ag compared to 3.3 ns on glass (PVA  $\sim$ 120 nm) and the average fluorescence lifetime of AMC is 2.1 ns in Al-PVA-Al compared to 3.4 ns on glass (PVA  $\sim$ 115 nm). The reduction in the fluorescence lifetimes on the MDM substrates is a favorable result because a fluorophore that spends less time in the excited state can undergo more excitation emission cycles prior to photo-decomposition. Thus, reduced fluorescence lifetime can

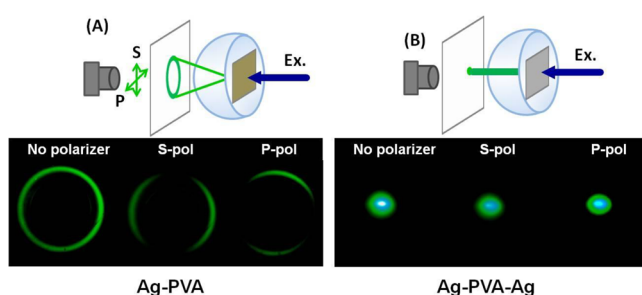


**Figure 12.** Illumination scheme (top panel) and real color photographs (bottom panel) of the fluorescence images of Fl projected on a screen for (A) Ag-PVA (cone-of-emission) and (B) Ag-PVA-Ag substrates (beaming emission) with a PVA thickness about 120 nm. The images were observed through a 500 nm long pass filter with either no emission polarizer, polarizer oriented vertically (S), or polarizer oriented horizontally (P).

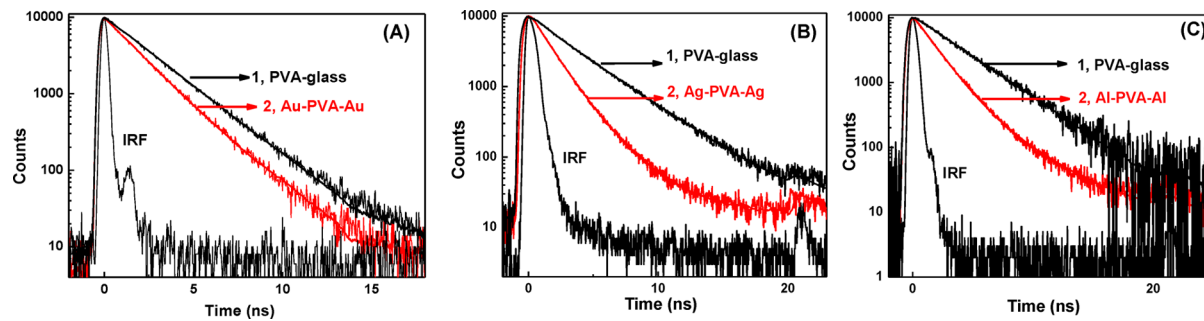


**Figure 13.** Fluorescence intensity decays of (A) NB in PVA-glass and Au-PVA-Au, PVA thickness  $\sim$ 160 nm; (B) Fl in PVA-glass and Ag-PVA-Ag, PVA thickness  $\sim$ 120 nm; (C) AMC in PVA-glass and Al-PVA-Al, PVA thickness  $\sim$ 115 nm. The intensity decays were collected close to  $180^\circ$ , corresponding to the beaming emission with these MDM substrates and were found to be independent of emission polarizer orientation (S or P).

improve the photostability of fluorophores in the MDM substrates. We found a modest increase in the nonexponential character of the decays in the MDM substrate. This effect is probably due to distance and orientation-dependent coupling of the fluorophores to the modes in the MDM structure. These results show that MDM structures can offer interesting opportunities for controlling molecular fluorescence. The coupling of fluorescence emission with the electromagnetic modes in these structures can be useful not only to steer the direction of fluorescence, but also to modify the excited state lifetimes of probes embedded within the MDM structures.

## CONCLUSION

This work shows that MDM structures of Au, Ag, or Al, fabricated using standard thermal deposition techniques, are capable of transforming the isotropic emission from randomly oriented fluorophores into directional emission. The type of metal and the dielectric layer thickness can be chosen according to the spectral range of the fluorophore. With Al, the range of wavelengths can be extended to the UV region while Au is more suitable for the NIR region. The spatial redistribution of emission in MDM structures occurs as a result of the channeling of fluorescence into electromagnetic modes present in the structure. For certain thicknesses of the dielectric layer and depending on the optical properties of the metals, the fluorescence emission can be obtained as a narrow beam normal to the MDM surface. Although in the present study we have considered symmetric MDM structures that are composed of the same metal in both the top and bottom layers, it will be possible to design MDM substrates with mixed metal layers to extend the optical response and mode properties of the structures. The distinct optical properties of individual metals will influence the radiation patterns of fluorophores in a manner different from that of a symmetric MDM substrate composed of the same metals. Bimetallic substrates, multilayers composed of solid films and nanoparticles, and Ag–Au nanocomposite structures are already being investigated by several groups including ours, for fluorescence enhancement studies and for improving the stability and biocompatibility of the substrates. We anticipate that similar benefits may be observed with MDM substrates composed of two different metals. The present study helps to strengthen our understanding of the coupling of fluorescence emission with MDM substrates and to benefit from the rich optical properties offered by these systems.

## AUTHOR INFORMATION

### Corresponding Author

\*E-mail: jlakowicz@umaryland.edu, sharmidc@barc.gov.in.

### Notes

The authors declare no competing financial interest.

## ACKNOWLEDGMENTS

S.D.C. acknowledges the Indo-US Science and Technology Forum (IUSSTF) for the grant of the IUSSTF Fellowship. This work was supported by NIH Grants HG002655, EB006521, and AI087968.

## REFERENCES

- 1) Orden, A. V.; Machara, N. P.; Goodwin, P. M.; Keller, R. A. Single-Molecule Identification in Flowing Sample Streams by Fluorescence Burst Size and Intraburst Fluorescence Decay Rate. *Anal. Chem.* **1998**, *70*, 1444–1451.
- 2) Köhn, F.; Hofkens, J.; Gronheid, R.; VanderAuweraer, M.; DeSchryver, F. C. Parameters Influencing the on- and Off-Times in the Fluorescence Intensity Traces of Single Cyanine Dye Molecules. *J. Phys. Chem. A* **2002**, *106*, 4808–4814.
- 3) Lal, S.; Link, S.; Halas, N. J. Nano-Optics from Sensing to Waveguiding. *Nat. Photonics* **2007**, *1*, 641–648.
- 4) Schuller, J. A.; Barnard, E. S.; Cai, W.; Jun, Y. C.; White, J. S.; Brongersma, M. L. Plasmonics for Extreme Light Concentration and Manipulation. *Nat. Mater.* **2010**, *9*, 193–204.
- 5) Bechger, L.; Lodahl, P.; Vos, W. L. Directional Fluorescence Spectra of Laser Dye in Opal and Inverse Opal Photonic Crystals. *J. Phys. Chem. B* **2005**, *109*, 9980–9988.
- 6) Rodriguez, S. R. K.; Lozano, G.; Verschueren, M. A.; Gomes, R.; Lambert, K.; De-Geyter, B.; Hassinen, A.; Van-Thourhout, D.; Hens, Z.; Gómez-Rivas, J. Quantum Rod Emission Coupled to Plasmonic Lattice Resonances: A Collective Directional Source of Polarized Light. *App. Phys. Lett.* **2012**, *100*, 111103.
- 7) Curto, A. G.; Volpe, G.; Taminiau, T. H.; Kreuzer, M. P.; Quidant, R.; Hulst, N. F. v. Unidirectional Emission of a Quantum Dot Coupled to a Nanoantenna. *Science* **2010**, *329*, 930–932.
- 8) Aouani, H.; Mahboub, O.; Bonod, N.; Devaux, E.; Popov, E.; Rigneault, H.; Ebbesen, T. W.; Wenger, J. Bright Unidirectional Fluorescence Emission of Molecules in a Nanoaperture with Plasmonic Corrugations. *Nano Lett.* **2011**, *11*, 637–644.
- 9) Aouani, H.; Mahboub, O.; Devaux, E.; Rigneault, H.; Ebbesen, T. W.; Wenger, J. Plasmonic Antennas for Directional Sorting of Fluorescence Emission. *Nano Lett.* **2011**, *11*, 2400–2406.
- 10) Jun, Y. C.; Huang, K. C. Y.; Brongersma, M. L. Plasmonic Beaming and Active Control over Fluorescent Emission. *Nat. Commun.* **2011**, *283*, 1–6.
- 11) Ding, B.; Hrelescu, C.; Arnold, N.; Isic, G.; Klar, T. A. Spectral and Directional Reshaping of Fluorescence in Large Area Self-

Assembled Plasmonic–Photonic Crystals. *Nano Lett.* **2013**, *13*, 378–386.

(12) Lakowicz, J. R. Radiative Decay Engineering 3. Surface Plasmon-Coupled Directional Emission. *Anal. Biochem.* **2004**, *324*, 153–169.

(13) Gryczynski, I.; Malicka, J.; Gryczynski, Z.; Lakowicz, J. R. Radiative Decay Engineering 4. Experimental Studies of Surface Plasmon-Coupled Directional Emission. *Anal. Biochem.* **2004**, *324*, 170–182.

(14) Gryczynski, I.; Malicka, J.; Nowaczyk, K.; Gryczynski, Z.; Lakowicz, J. R. Effects of Sample Thickness on the Optical Properties of Surface Plasmon-Coupled Emission. *J. Phys. Chem. B* **2004**, *108*, 12073–12083.

(15) Lakowicz, J. R.; Ray, K.; Chowdhury, M.; Szmacinski, H.; Fu, Y.; Zhang, J.; Nowaczyk, K. Plasmon-Controlled Fluorescence: A New Paradigm in Fluorescence Spectroscopy. *Analyst* **2008**, *133*, 1308–1346.

(16) Calander, N. Surface Plasmon-Coupled Emission and Fabry-Perot Resonance in the Sample Layer: A Theoretical Approach. *J. Phys. Chem. B* **2005**, *109*, 13957–13963.

(17) Cao, S.-H.; Cai, W.-P.; Liu, Q.; Li, Y.-Q. Surface Plasmon-Coupled Emission: What Can Directional Fluorescence Bring to the Analytical Sciences? *Ann. Rev. Anal. Chem.* **2012**, *5*, 317–336.

(18) Yuk, J. S.; Trnavsky, M.; McDonagh, C.; MacCraith, B. D. Surface Plasmon-Coupled Emission (Spce)-Based Immunoassay Using a Novel Paraboloid Array Biochip. *Biosens. Bioelectron.* **2010**, *25*, 1344–1349.

(19) Cao, S.-H.; Xie, T.-T.; Cai, W.-P.; Liu, Q.; Li, Y.-Q. Electric Field Assisted Surface Plasmon-Coupled Directional Emission: An Active Strategy on Enhancing Sensitivity for DNA Sensing and Efficient Discrimination of Single Base Mutation. *J. Am. Chem. Soc.* **2011**, *133*, 1787–1789.

(20) Xie, T.-T.; Liu, Q.; Cai, W.-P.; Chen, Z.; Li, Y.-Q. Surface Plasmon-Coupled Directional Emission Based on a Conformational-Switching Signaling Aptamer. *Chem. Commun.* **2009**, 3190–3192.

(21) Dutta Choudhury, S.; Badugu, R.; Nowaczyk, K.; Ray, K.; Lakowicz, J. R. Tuning Fluorescence Direction with Plasmonic Metal-Dielectric–Metal Substrates. *J. Phys. Chem. Lett.* **2013**, *4*, 227–232.

(22) Villa, F.; Lopez-Rios, T.; Regalado, L. E. Electromagnetic Modes in Metal-Insulator-Metal Structures. *Phys. Rev. B* **2001**, *63*, 165103–1–165103–4.

(23) CRC Handbook of Chemistry and Physics, 89th ed.; Taylor & Francis Group: Boca Raton, 2008.

(24) Gryczynski, I.; Malicka, J.; Gryczynski, Z.; Nowaczyk, K.; Lakowicz, J. R. Ultraviolet Surface Plasmon-Coupled Emission Using Thin Aluminum Films. *Anal. Chem.* **2004**, *76*, 4076–4081.

(25) Gryczynski, I.; Malicka, J.; Gryczynski, Z.; Lakowicz, J. R. Surface Plasmon-Coupled Emission with Gold Films. *J. Phys. Chem. B* **2004**, *108*, 12568–12574.

(26) Becker, H.; Burns, S. E.; Tessler, N.; Friend, R. H. Role of Optical Properties of Metallic Mirrors in Microcavity Structures. *J. Appl. Phys.* **1997**, *81*, 2825–2829.

(27) Becker, H.; Friend, R. H.; Wilkinson, T. D. Light Emission from Wavelength-Tunable Microcavities. *Appl. Phys. Lett.* **1998**, *72*, 1266–1268.

(28) Purcell, E. M. Spontaneous Emission Probabilities at Radio Frequencies. *Phys. Rev.* **1946**, *69*, 681.